THE PROTEIN SOCIETY

Intersubunit communication in the dihydroorotase–aspartate transcarbamoylase complex of *Aquifex aeolicus*

Hedeel Guy Evans,[1,2] Roshini Fernando,[1] Asmita Vaishnav,[2] Mahalakshmi Kotichukkala,[1] Deborah Heyl,[1] Fatme Hachem,[2] Joseph S. Brunzelle,[3] Brian F.P. Edwards,[2] and David R. Evans[2]*

[1]Department of Chemistry, Eastern Michigan University, Ypsilanti, Michigan 48197
[2]Department of Biochemistry and Molecular Biology, Wayne State University, School of Medicine, Detroit, Michigan 48201
[3]Life Sciences Collaborative Access Team, Northwestern University, Center for Synchrotron Research, Argonne, Illinois 60439

Received 8 September 2013; Revised 1 November 2013; Accepted 1 November 2013
DOI: 10.1002/pro.2396
Published online 7 November 2013 proteinscience.org

Abstract: Aspartate transcarbamoylase and dihydroorotase, enzymes that catalyze the second and third step in *de novo* pyrimidine biosynthesis, are associated in dodecameric complexes in *Aquifex aeolicus* and many other organisms. The architecture of the dodecamer is ideally suited to channel the intermediate, carbamoyl aspartate from its site of synthesis on the ATC subunit to the active site of DHO, which catalyzes the next step in the pathway, because both reactions occur within a large, internal solvent-filled cavity. Channeling usually requires that the reactions of the enzymes are coordinated so that the rate of synthesis of the intermediate matches its rate of utilization. The linkage between the ATC and DHO subunits was demonstrated by showing that the binding of the bisubstrate analog, *N*-phosphonacetyl-L-aspartate to the ATC subunit inhibits the activity of the distal DHO subunit. Structural studies identified a DHO loop, loop A, interdigitating between the ATC domains that would be expected to interfere with domain closure essential for ATC catalysis. Mutation of the DHO residues in loop A that penetrate deeply between the two ATC domains inhibits the ATC activity by interfering with the normal reciprocal linkage between the two enzymes. Moreover, a synthetic peptide that mimics that part of the DHO loop that binds between the two ATC domains was found to be an allosteric or noncompletive ATC inhibitor (K_i = 22 μM). A model is proposed suggesting that loop A is an important component of the functional linkage between the enzymes.

Keywords: aspartate transcarbamoylase; CAD; dihydroorotase; metabolic channeling; pyrimidine biosynthesis; thermophile; intersubunit communication; *N*-phosphonacetyl-L-aspartate; linkage; allosteric regulation

Abbreviations: ATC, aspartate transcarbamoylase; CAD, a polypeptide chain present in mammals and some other species that includes the first three enzymes of pyrimidine biosynthesis; CP, carbamoyl phosphate; Casp, carbamoyl aspartate; DAC, the dodecameric complex consisting of six copies of ATC and six copies of DHO; DHO, dihydroorotase; dho, dihydroorotate; PALA, N-phosphonacetyl-L-aspartate

Grant sponsors: NIH: HL57527, GM47399, GM/CA60371. NSF: MCB9810325. Michigan Economic Development Corporation: 085P1000817. U.S. Dept. of Energy: W-31-109-Eng-38, DE-AC02-06CH11357. X-ray data were collected at LS-CAT supported by the MEDC at sector 21 of the Advanced Photon Source, which is a DOE Office of Science User Facility Operated by Argonne National Laboratory.

*Correspondence to: David R. Evans; Department of Biochemistry and Molecular Biology, Wayne State University School of Medicine, 540 E. Canfield St., Detroit, MI 48201.
E-mail: drevans@med.wayne.edu

Introduction

Aspartate transcarbamoylase (ATC) and dihydroorotase (DHO) catalyze the second and third steps in the *de novo* pyrimidine biosynthetic pathway.[1] These reactions (Scheme 1) occur almost universally in all organisms.

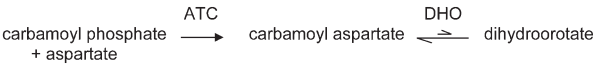

Scheme 1. Reactions catalyzed by *A. aeolicus* DAC.

In mammalian cells, the first three steps of the *de novo* pyrimidine pathway are consolidated in a hexamer consisting of a single 243 kDa polypeptide chain called CAD so named for the constituents, **c**arbamoyl phosphate synthetase, aspartate transcarbamoylase, and dihydroorotase. Multifunctional pyrimidine biosynthetic complexes are found only in eukaryotes, but the corresponding enzymes in many, but not all, prokaryotes associate to form multienzyme complexes. In *Aquifex aeolicus*, a prokaryotic organism of ancient lineage,[2] ATC forms a stoichiometric complex with DHO consisting of six copies of each enzyme.[3] Moreover, there is kinetic evidence suggesting that carbamoyl phosphate synthetase, which catalyzes the preceding step in the pathway, forms a transient complex with ATC[4] that allows the direct transfer of carbamoyl phosphate to ATC.

The *A. aeolicus* DHO-ATC dodecameric complex [DAC, Fig. 1(A)] consists of two trimeric ATC subunits and three DHO dimers.[3] The subunits are arranged[5] to enclose a large, aqueous-filled central cavity [Fig. 1(B)]. Remarkably, the active sites of both enzymes face the interior of the central cavity. The only access to the cavity is via six narrow intersubunit tunnels. The structural organization of the complex promotes the direct transfer or channeling of carbamoyl aspartate from the active site of the ATC subunit to the active site of the DHO subunit.

Channeling is especially advantageous for the DAC complexes because the conversion of carbamoyl aspartate to dihydroorotate is rapidly reversible with the equilibrium strongly favoring carbamoyl aspartate by a factor of 17 at physiological pH.[6] Moreover, the apparent second-order rate constant (k_{cat}/K_m) of ATC is 7.0-fold greater than that of DHO.[4] The structural organization of the *A. aeolicus* DAC complex ensures that carbamoyl aspartate does not accumulate at high concentrations in the cytoplasm and that once released from the interior cavity of the complex, dihydroorotate is not converted back to carbamoyl aspartate. The channeling of metabolic intermediates usually involves coordination of the activities of enzymes catalyzing consecutive reactions.[7–9] Thus, the transfer of carbamoyl aspartate from its site of synthesis on ATC to the active site of DHO is likely to require a functional linkage between the enzymes that matches its rate of formation to its rate of utilization.

The catalytic subunits of *Escherichia coli*[10,11] and *A. aeolicus* ATC (unpublished result) have similar amino acid sequences, domain structure, and tertiary fold and are likely to proceed via the same catalytic mechanism. *E. coli* ATC is a dodecameric monofunctional protein that is not associated with any other enzyme in the pyrimidine biosynthetic pathway.[12] Like the *E. coli* catalytic subunit, *A. aeolicus* ATC is a trimer consisting of a carbamoyl phosphate binding domain and an aspartate binding domain [Fig. 1(C)]. Upon binding of the substrates or the bisubstrate analog, *N*-phosphonacetyl-L-aspartate

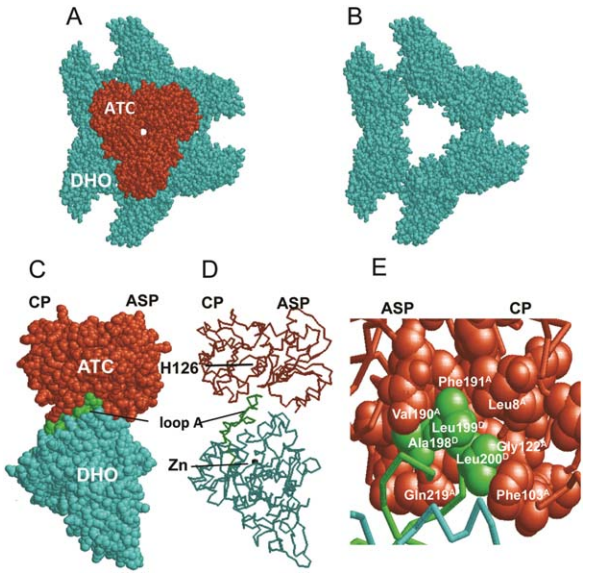

Figure 1. Structure of the DAC complex. (A) The intact DAC dodecamer showing the arrangement of subunits. The ATC subunits associate to form two trimers, one on the front in this view and the other hidden behind the structure. The DHO subunits are associated as a peripheral ring consisting of three DHO dimers. (B) The large central cavity of the complex (diameter 65 Å) can be seen if the front and back ATC trimers that cap the cavity, are removed. (C) A space-filled view, perpendicular to the three-fold axis, of one ATC monomer with its constituent carbamoyl phosphate binding domain (CP) and aspartate binding domain (ASP) is shown bound to the nearest DHO monomer. The loop on the DHO domain, loop A interdigitates between the two ATC domains. (D) The backbone of the same ATC-DHO pair as in C, showing loop A, the active site histidine, His126, on the ATC subunit and the Zn at the active site of DHO. The distance between the active sites is approximately 14 Å. (E) Three hydrophobic residues of loop A, Ala198^D, Leu199^D and Leu200^D (space filled) are wedged between the two ATC domains; the CP domain, residues 1-150 and the ASP domain, residues 151-304. Most of the loop A neighbors, (space filled) on the ATC domain are hydrophobic. Superscripts A and D indicate residues on the ATC and DHO subunits, respectively. The figure was composed with RasWin using the structural coordinates[5] deposited in the Protein Data Bank (PDB Id: 3B6N).

(PALA), there is a reorientation of the carbamoyl phosphate and aspartate domains from the open, accessible conformation in the unliganded enzyme to a closed form in which the bound substrates or analogs are completely buried.[11,13] Domain closure is an essential step in the catalytic cycle, but in the structure of the *A. aeolicus* DAC complex,[5] there is a flexible loop, loop A, on the DHO subunit that interdigitates between the ATC subdomains [Fig. 1(C,D)] that might be expected to interfere with domain closure.

This study was undertaken to determine whether the ATC and DHO subunits of the *A. aeolicus* complex are functionally coupled and whether the loop A on the DHO subunit can modulate the activity of the ATC subunit.

Results

Functional coupling of enzymes that catalyze consecutive reactions occurs when events, such as the binding of substrates or inhibitors, to one enzyme modulates the activity of the next enzyme in the reaction sequence. In the case of the *A. aeolicus* DAC complex, we assessed the effect of the binding of the potent ATC inhibitor, PALA, on the catalytic activity of the DHO component of the complex.

Effect of PALA on the dihydroorotase activity

PALA, a bisubstrate analog of the ATC substrates, carbamoyl phosphate and aspartate, is a highly specific inhibitor of ATC[14] from all organisms, including the *A. aeolicus* enzyme.[4] The inhibitor binds tightly and specifically to the ATC active site[14] but has no affinity for the active site of the DHO subunit. To determine whether the catalytic activities of the ATC and DHO subunits are functionally linked, the DHO saturation curve using dihydroorotate as the variable substrate was determined for the DAC complex (Fig. 2) at several different concentrations of PALA ranging from 1 n*M* to 1 m*M*. The experiment clearly shows that PALA strongly inhibited the DHO activity of the complex. The K_m of the DHO catalyzed reaction increased only slightly with increasing concentrations of the inhibitor (Table I). In contrast, the V_{max} decreased progressively with 82% inhibition observed at 1 m*M* PALA. A least squares fit gave a K_i of 6.21 ($\pm$1.62) $\times$ 10^{-10} *M* for the noncompetitive inhibition of the DHO activity. This value was 440-fold lower than the K_i value for the competitive inhibition of *E. coli* ATC by PALA obtained using carbamoyl phosphate as the variable substrate.[14] The K_i (noncompetitive) for DHO inhibition would be appreciably higher had carbamoyl phosphate, which competes with PALA at the ATC active site, been present in the assay.

Extensive structural and kinetic studies have shown that PALA binding to *E. coli* ATC stabilizes the closed form of the catalytic subunit.[13,15,16] These results strongly suggest that domain closure of the ATC subunit induced by PALA results in inhibition of the activity of the DHO subunit of the *A. aeolicus* complex, an indication that the catalytic activities are functionally linked.

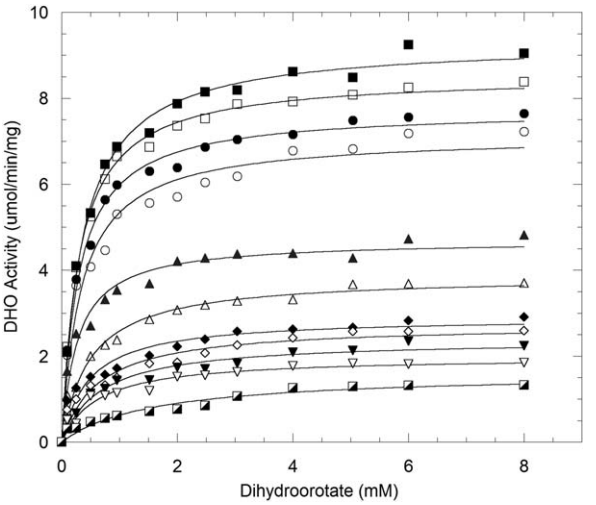

Figure 2. The effect of PALA bound to ATC on the activity of DHO. The DAC complex[3] was formed by mixing stoichiometric amounts of the purified *Aquifex aeolicus* DHO[25] and ATC.[4] The dihydroorotate saturation curves of the DHO subunit were determined at different concentrations of the potent ATC inhibitor, PALA; no PALA (■); 0.1 n*M* PALA (□); 0.25 n*M* (●); 0.50 n*M* (○); 1 n*M* (▲), 1 μ*M* (△); 2.5 μ*M* (◆); 5 μ*M* (◇); 10 μ*M* (▼); 100 μ*M* (▽); 1 m*M* (◪). The assays were performed as described in Materials and Methods, with 40 μg of DHO and 29.6 μg of ATC for each determination.

Structural interactions between the ATC and DHO subunits

The isolated DHO subunit is catalytically inactive and the X-ray structure shows there are three loops, designated loops A, B, and C that are largely disordered.[15] A short segment of loop A is visible in the electron density map and has a cysteine residue, Cys180 that can serve as a zinc ligand effectively blocking the binding of substrates to the DHO active

Table I. *Effect of PALA on the DHO Kinetic Parameters[a] of DAC*

PALA M	K_m mM	V_{max} μmol/min/mg
0	0.355 ± 0.023	9.23 ± 0.11
0.10×10^{-9}	0.293 ± 0.013	8.53 ± 0.07
0.25×10^{-9}	0.292 ± 0.021	7.73 ± 0.11
0.50×10^{-9}	0.336 ± 0.048	7.13 ± 0.19
1.0×10^{-9}	0.268 ± 0.038	4.94 ± 0.12
1.0×10^{-6}	0.491 ± 0.058	3.85 ± 0.10
2.5×10^{-6}	0.471 ± 0.092	2.90 ± 0.12
5.0×10^{-6}	0.630 ± 0.116	2.72 ± 0.12
1.0×10^{-5}	0.671 ± 0.107	2.38 ± 0.09
1.0×10^{-4}	0.619 ± 0.107	1.97 ± 0.08
1.0×10^{-3}	1.57 ± 0.337	1.61 ± 0.12

[a] Determined by a least squares fit of the data shown in Figure 1 to the Michaelis–Menten equation.

site. Upon formation of the DAC complex, there is a reorganization of loops A, B, and C to form the interface between the DHO and ATC subunits.[5] Loop A is especially interesting in that it deeply extends between the carbamoyl phosphate and aspartate domains and would be expected to interfere with domain closure [Fig. 1(C,D)].

Loop A mutations

The structure of the DAC complex [Fig. 1(E)] showed that three hydrophobic residues, Ala198^D, Leu199^D, and Leu200^D of loop A on the DHO subunit interdigitate deeply between the two ATC domains. The loop is in close proximity to both ATC domains, the carbamoyl phosphate-binding domain (CP domain, residues 1–139) and the aspartate-bonding domain (ASP domain, residues 150–304) in a region of the cleft that is also hydrophobic.

Three mutants were constructed, Ala198Arg^D, Leu199Arg^D, and Leu200Arg^D (Materials and Methods), to investigate the role of the three loop residues in the functional linkage. In each case, the hydrophobic residue was replaced by a bulky, positively charged residue that would be expected to dislodge the loop from the interdomain cleft and disrupt the intersubunit communication.

Kinetics of loop A mutants

Carbamoyl phosphate saturation curves [Fig. 3(A)] of the mutant DAC complexes showed that replacement of Ala198, Leu199, and Leu200 with arginine had little effect on the ATC activity of DAC. In contrast, the dihydroorotate saturation curves [Fig. 3(B)] of the DAC complexes reconstituted with the native ATC subunits and the mutant DHO subunits showed that the mutations resulted in a substantial decrease in the V_{max}, but had little effect on the dihydroorotate K_m (Table II). Because the isolated DHO is inactive, a reduced V_{max} for the mutants could be explained if the mutations blocked the association of the ATC and DHO subunits.

All three mutations weakened the intersubunit interactions between the DAC subunits. The wild-type DHO is only active when it is physically associated with ATC in the DAC complex,[3] so DHO activity can be used to assess complex formation as a fixed amount of the ATC subunit is titrated with the mutant DHO [Fig. 4(A)]. For the wild-type DHO, the maximum activity was observed at a molar ratio of DHO/ATC of approximately 1.0. Continued addition of the DHO did not result in increased DHO activity because there was insufficient ATC to activate its latent activity.

In contrast, titration of ATC with the Leu200Arg mutant had an endpoint corresponding to a molar ratio of DHO/ATC of approximately five, indicative of much weaker intersubunit interactions. Moreover,

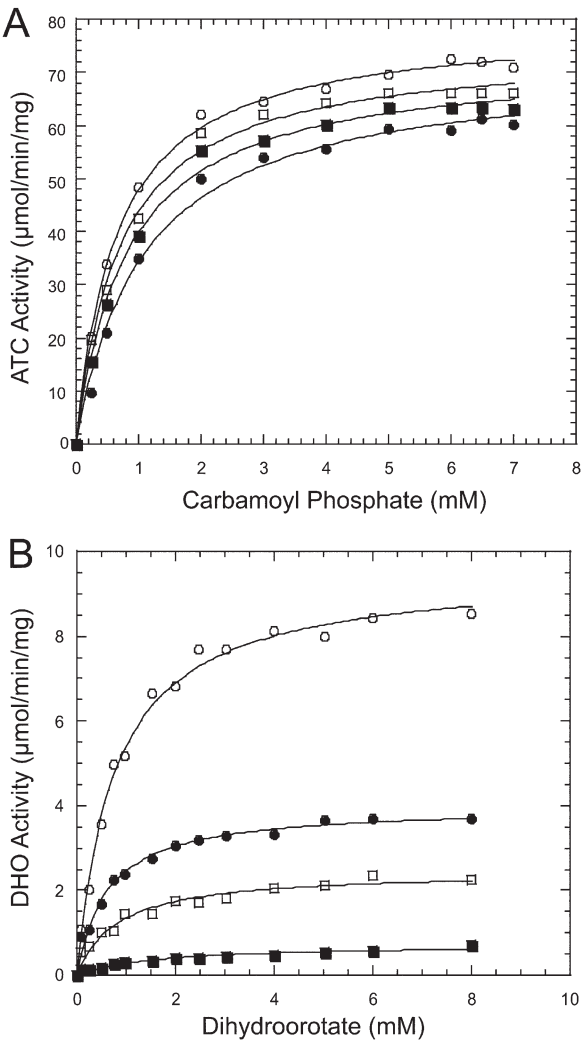

Figure 3. Steady state kinetics of DHO loop A mutants. (A) the carbamoyl phosphate saturation curve of the ATC component of DAC reconstituted with wild-type ATC and the wild-type DHO (○) and the DHO mutants, Leu200Arg (●), Leu199Arg (□), and Ala198Arg (■). (B) The dihydroorotate saturation curve of the DHO component of DAC reconstituted with the wild-type ATC and the mutant DHO subunits (same symbols).

when the ATC subunit was completely saturated, the DHO activity of the mutant was reduced by 48%, a value consistent with the reduction in V_{max} obtained from the saturation curve [Fig. 3(B)]. The Leu199Arg

Table II. *DHO Steady State Kinetic Parameters[a] of the DHO Mutants*

	V_{max}	K_m
Protein	μmol/min/mg	mM
Wild type	9.53 ± 0.17	0.763 ± 0.05
Leu200Arg	3.98 ± 0.09	0.621 ± 0.06
Leu199Arg	2.45 ± 0.11	0.81 ± 0.13
Ala198Arg	0.73 ± 0.59	1.59 ± 0.36

[a] Determined by a least squares fit of the data shown in Figure 2 to the Michaelis–Menten equation.

mutant was more drastically affected with an endpoint of DHO/ATC of four and 75% inhibition of the DHO activity at saturating DHO.

Although both the Leu199Arg and Leu200Arg mutants associated with ATC and retained catalytic activity, albeit impaired, no activation of the Ala198Arg mutant was observed at any concentration of ATC up to a molar ratio of DHO/ATC of 25:1, suggesting that this DHO mutant cannot associate with ATC. This interpretation was confirmed by gel filtration [Fig. 4(B)]. Although the wild-type DAC complex eluted from the column as a single homogenous peak having both ATC and DHO activities, the Ala198Arg mutant gave two distinct peaks when analyzed by measuring the absorbance at 280 nm (not shown) and by SDS polyacrylamide gel electrophoresis. The stained SDS gel showed that the molecular mass of these two species was 49 and 37 kDa corresponding to the DHO and ATC subunits, respectively. The 37 kDa peak had strong ATC activity, whereas the 49 kDa peak was catalytically inactive. This result might be expected because Ala198 was replaced with a much bulkier and highly charged Arg residue and because this residue is completely buried within the subunit interface [Fig. 1(E)], whereas Leu199 and Leu200 are more solvent accessible.

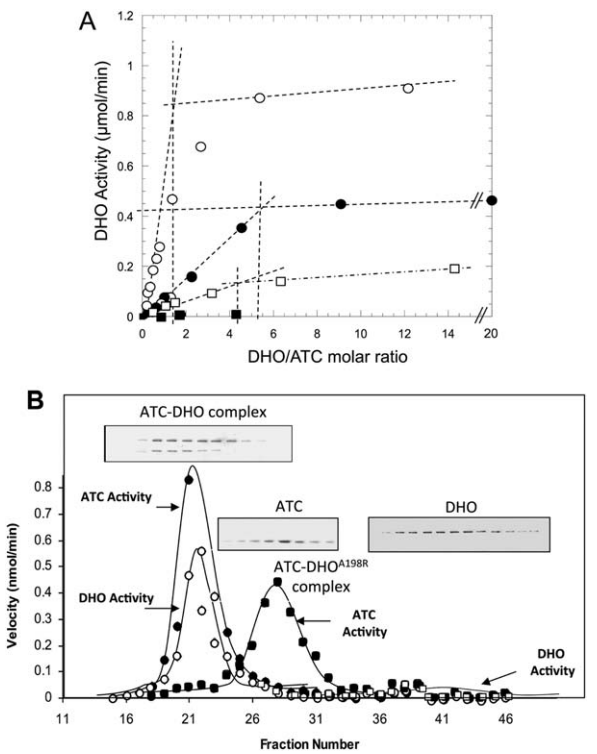

Figure 4. Titration of ATC with wild-type and DHO mutants. (A) The isolated ATC subunit (7 μg) was titrated with wild-type DHO (○) and the Leu200Arg (●), Leu199Arg (□), and Ala198Arg (■) mutants and the DHO activity was assayed. The DHO subunit is active only when present in a complex with ATC, so the endpoint corresponds to the molar ratio at saturation when all of the ATC is complexed to DHO. (B) Sephacryl S-300 gel filtration of the native DAC complex shows a single high molecular weight peak as determined by the absorbance at 280 nm (not shown) and SDS gel electrophoresis (inset). The peak has a 37 kDa ATC subunit and 49 kDa DHO subunit and both ATC (●) and DHO (○) activities. The Ala198Arg mutant column profile has two distinct peaks as determined by absorbance. The first peak consists of the 37 kDa ATC subunit and has ATC activity (■) whereas the second peak contains only the inactive DHO subunit.

Although the inability of the DHO Ala198Arg mutant to associate with the ATC subunit precludes any conclusions regarding the role of this residue in the functional linkage, both the Leu199Arg and Leu200Arg mutants did associate with the ATC subunit. However, the DHO activity was significantly lower even at higher concentrations where there was sufficient DHO to saturate the ATC subunit. These results indicate that the interaction of DHO loop A with the ATC subunit plays an important role in the intersubunit communication.

Effect of a synthetic loop A peptide on ATC activity

The question becomes, does the presence of loop A wedged between the carbamoyl phosphate and aspartate domains of ATC modulate its catalytic activity? To answer this question, a peptide was synthesized (*Materials and Methods*) corresponding to the segment of loop A (DHO residues 192-203) of the DHO subunit that extends between the ATC domains (*Scheme* 2).

The isolated ATC subunit was progressively inhibited by increasing concentrations of the peptide [Fig. 5(A)] suggesting that it was interfering with domain closure and thus catalysis. The activity was inhibited by 96% at the highest concentration of peptide tested. The effect of the peptide on the ATC activity of the DAC complex was significantly smaller, presumably because access to the ATC site that binds the peptide is restricted by the binding of loop A on the DHO subunit of the DAC complex. The DHO activity of the complex is also inhibited by the peptide [Fig. 5(B)] but this is likely to be an indirect effect due to the inhibition of the ATC component, because the association with the ATC subunit is necessary for DHO activation. As expected,[3] the isolated DHO lacks catalytic activity at all concentrations of the peptide tested.

Carbamoyl phosphate saturation curves of the isolated ATC subunit were conducted at several concentrations of the peptide [Fig. 6(A), Table III]. A least squares analysis showed that although the peptide had little effect on the K_m for carbamoyl

DHO loop A	179	DHCEDDKLAYGVINEGEVS**ALL**GLSSRAPEAE 210
Synthetic peptide	192	NEGEVS**ALL**GLS 203

Scheme 2. Sequence of loop A and the peptide inhibitor.

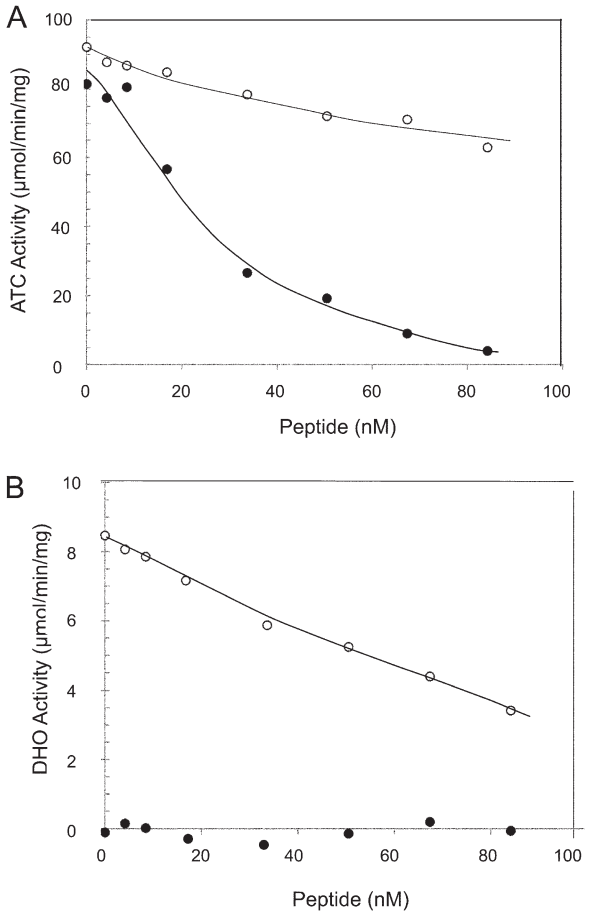

Figure 5. The effect of Peptide on the activities of DAC. (A) The ATC activity of the isolated ATC subunit (●) and of DAC (○) was assayed as a function of the peptide concentration. (B) The DHO activity of DAC (○) and the isolated DHO subunit (●) was also assayed at the indicated concentration of the peptide.

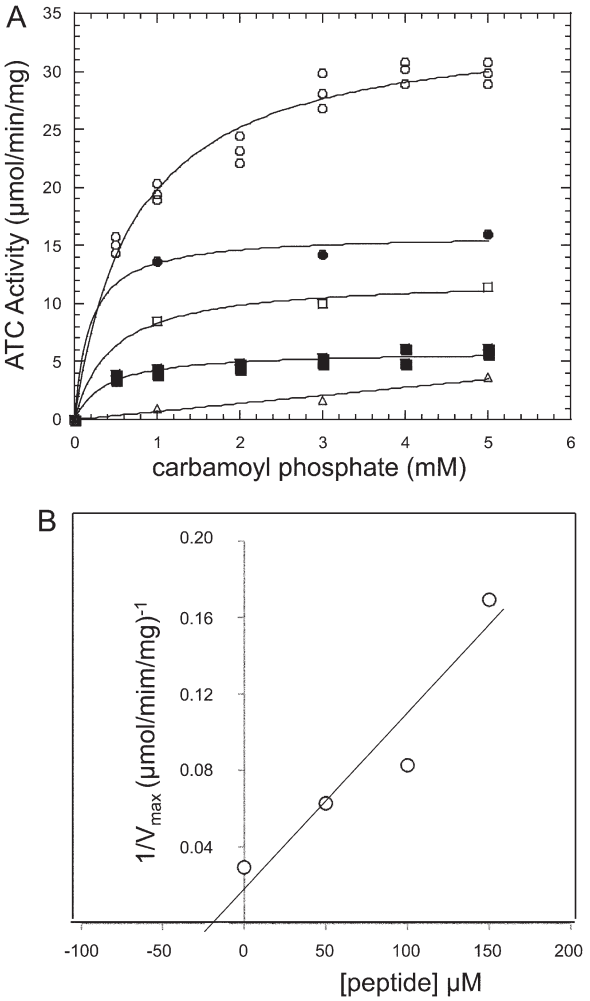

Figure 6. Steady state kinetics of the ATC subunit at various concentrations of the peptide. (A) Carbamoyl phosphate saturation curves were determined in the absence of the peptide (○) and at 50 μ*M* (●), 100 μ*M* (□), 150 μ*M* (■) and 250 μ*M* (△) peptide concentrations. The data were fit to the Michaelis–Menton equation and the steady state kinetic parameters are summarized in Table III. (B) The inhibition constant K_i was determined to be 22 μ*M* from a plot of $1/V_{max}$ versus the peptide concentration.

phosphate, there was a significant decrease in the V_{max}, suggesting that the peptide is a noncompetitive inhibitor. Consistent with this interpretation, a replot of the reciprocal V_{max} versus the concentration of peptide [Fig. 6(B)] is linear with a K_i = 22 μM. Thus, assuming that the anticipated X-ray structure currently underway verifies the expected binding site of the peptide, the intercalation of the peptide between the ATC domains probably interferes with domain closure that is an essential part of the ATC catalytic cycle.

Discussion

Although the active sites of the two enzymes that comprise the DAC complex are approximately 14 Å apart, their activities are functionally coupled. The binding of the bisubstrate analog PALA to the active site of ATC strongly inhibits the activity of the DHO subunit. The inhibition affects the V_{max} with little effect on the K_m except at the highest concentration (1 m*M*) PALA. As is typical for this type of allosteric effect, the inhibition seems to be incomplete decreasing the activity to about 82%. The low K_i for DHO inhibition (6.21×10^{-10} *M*) by PALA indicates that the effect of the inhibitor, designed as an ATC bisubstrate or transition state analog,[14] on the DHO

Table III. *ATC Kinetic Parameters[a] in the Presence of Peptide*

Peptide	V_{max}	K_m
μM	μmol/min/mg	mM
0	34.3 ± 0.87	0.73 ± 0.07
50	15.9 ± 0.81	0.19 ± 0.10
100	12.1 ± 0.59	0.46 ± 0.13
150	5.90 ± 0.28	0.38 ± 0.10

[a] Determined by a least squares fit of the data shown in Figure 2(A) to the Michaelis–Menten equation.

activity is a direct consequence of the binding of PALA to the ATC subunit.

In enzyme systems that channel metabolic intermediates, there is typically a reciprocal linkage between reactions occurring at the different active sites.[9] The sequential reactions are coordinated such that the formation of the product by the first enzyme matches its rate of utilization by the second enzyme. For example, *E. coli* tryptophan synthetase, a bifunctional enzyme comprised of α and β subunits, catalyzes the last two steps of the tryptophan biosynthetic pathway. There is an intramolecular tunnel for the transfer of the intermediate, indole, formed on the α subunit, to the site of synthesis of tryptophan on the β subunit.[16] The formation of indole on the α subunit is slow unless the aminoacrylate is first formed from L-serine on the β subunit.[17] Similarly, carbamoyl phosphate synthetase has three distinct active sites connected by a long intramolecular tunnel.[18] The partial reactions are synchronized by allosteric communication between active sites.[19,20] In *de novo* pyrimidine biosynthesis in *A. aeolicus*, carbamoyl phosphate synthetase, which catalyzes the first step in the pathway, forms a transient complex with ATC, that channels carbamoyl phosphate between the active sites.[4] The second and third reactions of the pathway in *A. aeolicus* occur in a large internal cavity within the stable DAC complex of ATC and DHO subunits. The synchronization of the reactions in the DAC complex is especially important because the intrinsic k_{cat} of the first enzyme, ATC, is 10-fold higher than that of the second enzyme and because the equilibrium is so unfavorable for dihydroorotate formation. The allosteric inhibition of the DHO activity by the binding of substrate analogs to the ATC subunit is one mechanism for the coordination of these reactions. The effect of mutations and synthetic loop A peptide analogs, described here, suggests that loop A plays a role in phasing the reactions. Mutations that disrupt the interactions between loop A and the ATC subunit seem to disrupt the linkage necessary for the activation of the DHO subunit. Moreover, a short peptide that mimics the region of loop A in DHO that interacts with ATC is a noncompetitive, allosteric inhibitor that interferes with the domain closure necessary for ATC catalysis.

A reciprocal linkage of a different sort has been observed to occur between the two monomers in the monofunctional *E. coli* DHO dimer. X-ray structures of the *E. coli* enzyme[21,22] have shown that one monomer has dihydroorotate bound, whereas carbamoyl aspartate is bound to the other monomer. It was subsequently found[23] that the active site occupied by dihydroorotate is an open conformation, whereas in the monomer with bound carbamoyl aspartate, a flexible loop moves toward the active site forming hydrogen bonds with the bound substrate.

We propose an analogous model involving reciprocal activation and inhibition of the ATC and DHO that could account in part for the coupling of the two reactions catalyzed by the DAC complex (Fig. 7). This scheme assumes that both the ATC and DHO subunits can exist in either an open or closed conformation. The substrate binds to the open conformation and induces closure and catalysis. Upon completion of the catalytic cycle, the active site opens and the products are released. The closed conformation of the ATC subunit in both the *E. coli* and *A. aeolicus* enzymes involves domain closure that completely sequesters the bound substrates. Similarly, in *E. coli* DHO, there is a flexible loop that covers the bound carbamoyl aspartate resulting in a closed conformation.[22,23] The corresponding loop does not exist in the *A. aeolicus* enzyme, so that the postulated conformational changes that occur upon substrate binding must be more subtle and are as yet undetermined.

In this scheme (Fig. 7), the active site of ATC in DAC, initially in an open conformation (not shown), closes upon the binding of substrates, carbamoyl phosphate and aspartate (A^c) and catalysis occurs. At this point, the active site of the DHO subunit is open (D^o) poised to bind the ATC product, carbamoyl aspartate (Casp). When carbamoyl aspartate is formed, the ATC active site opens, releasing the intermediate which diffuses within the central cavity to the active site of the DHO subunit. With the release of carbamoyl aspartate, a conformational change causes loop A to interdigitate between the ATC domains inhibiting another round of ATC catalysis. The binding of carbamoyl aspartate to the DHO active site induces its "closed conformation" and dihydroorotate (dho) is formed. Upon formation of dihydroorotate, the DHO active site opens and the product is released. At the same time, Loop A undergoes a conformational change, perhaps analogous to its disordered conformation in the inactive, isolated DHO subunit,[3,15] that dislodges it from the interdomain cleft between the ATC domains allowing another round of carbamoyl aspartate formation.

This model can account for the inhibition of DHO activity by PALA. When PALA is bound to ATC, no catalysis occurs and the ATC active site remains in the closed conformation. The reciprocal linkage between the ATC and DHO sites would result in the concomitant inhibition of the DHO activity because the DHO would be locked in the open conformation and could not undergo catalysis.

Proof of this hypothesis will require additional biochemical and structural studies. The current DAC structure was determined with citrate bound to both the ATC and DHO active sites.[5] If the proposed scheme has merit, the structure of DAC without bound ATC substrates or substrate analogs would be expected to show an open conformation for

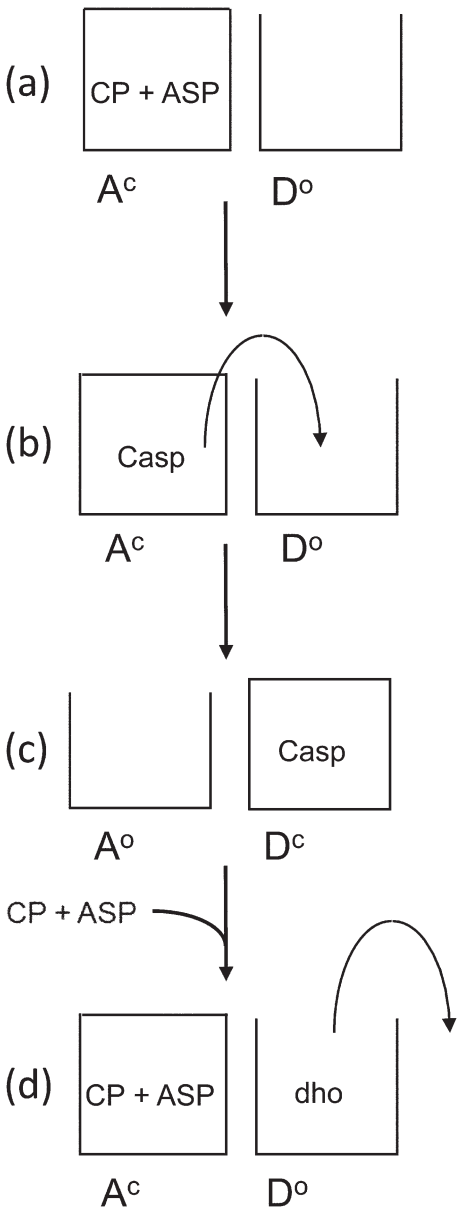

Figure 7. Proposed model for the reciprocal coupling of the ATC and DHO subunits of DAC. Both ATC and DHO can exist in an open conformation (superscript o) that can bind substrates and a closed conformation (superscript c) where catalysis occurs. The coupling is reciprocal in that when the ATC domain is closed, the DHO domain is open and vice versa. (a) The binding of carbamoyl phosphate (CP) and aspartate (ASP) induces domain closure of the ATC subunit (A^c). The DHO remains in the open conformation (D^o). (b) carbamoyl aspartate (Casp) is formed. (c) The ATC subunit opens and carbamoyl aspartate (Casp) is released and diffuses to the DHO active site, which then closes in turn (D^c). The open conformation of ATC binds CP and ASP in preparation of another round of catalysis. (d) The conversion of Casp to dihydroorotate (dho) results in the opening of the DHO domain (D^o) and the release of the final product.

ATC with loop A interdigitating between the two domains, whereas the DHO would be expected to be in the closed conformation. In the DAC PALA structure, the binding of PALA to ATC would be expected to displace loop A allowing ATC domain closure. The DHO would be in an open conformation and cannot undergo closure or catalysis. Determination of these structures is currently underway. Although the coupling mechanism remains to be fully elucidated, the results described here suggest that the interdigitation of loop A between the carbamoyl phosphate and aspartate domains of ATC is a key element of the linkage.

Materials and Methods

Materials

All chemicals were purchased from Sigma-Aldrich. *E. coli* strains DH5α and BL21 (DE3) were from Invitrogen. For peptide synthesis, all of the protected amino acids were purchased from Bachem Americas (Torrance, CA), Anaspec (Freemont, CA), and Synthetech (Albany, OR). Coupling agents and resins were purchased from Bachem Americas and Midwest Biotech (Fishers, IN). Solvents and deprotecting agents were obtained from Fisher Scientific (Pittsburgh, PA) and Sigma-Aldrich Chemical Co. (St. Louis, MO).

Isolation of the DHO and ATC subunits and formation of the DAC complex

The genes encoding *A. aeolicus* DHO (*pyrC*) and ATC (*pyrB*) subunits were previously cloned and separately expressed in *E. coli*.[3,4,15,25] The genes were identified in the *A. aeolicus* genome,[2] amplified by PCR and inserted into pRSETC (Invitrogen), an expression vector that incorporates a 3-kDa His tag on the amino end of the recombinant protein. The proteins were expressed individually in BL21 (DE3) and purified by Ni^{+2} affinity chromatography on a 1-mL Ni^{+2} Probond column (Invitrogen). The purified subunits were mixed in an equimolar ratio to reconstitute the dodecameric DHO-ATC complex.[3] The complex was isolated by gel filtration chromatography on a Sephacryl S-300 column. The composition of the complex was analyzed by SDS polyacrylamide gel electrophoresis[25,26] and ATC and DHO assays. Protein concentrations were determined by the Lowry method[26,27] using bovine serum albumin as a standard.

Enzyme assays

The activity of the ATC subunit was measured at 75°C by the colorimetric method previously described[4] before reconstituting the DHO-ATC complex to insure that the subunit was fully functional. The reaction contained 2 m*M* aspartate, 5 m*M* carbamoyl phosphate, 1-11 μg of the purified enzyme, and 50 m*M* Tris-HCl, pH 8, in a total volume of 0.5 mL. A short reaction time, 1.5 min, was necessitated because of the instability of carbamoyl phosphate, which is rapidly degraded at elevated temperature

(k_d = 0.74 min^{-1} at 70°C).[4] At 5 m*M* carbamoyl phosphate, ATC remains essentially saturated throughout the course of the assay. The reactions were quenched by the addition of an equal volume of 5% acetic acid. The color was developed and quantitated as described previously.[27,28]

DHO activity was measured in the reverse direction, the formation of carbamoyl aspartate from dihydroorotate, because the equilibrium strongly favors dihydroorotate hydrolysis under these conditions. The formation of carbamoyl aspartate was measured using the same colorimetric method. The assay mixture, consisting of 20–45 μg DHO in 50 m*M* Tris acetate, pH 8.3, 10% glycerol, was preincubated for 1.5 min at 75°C. The reaction was initiated by the addition of dihydroorotate (8 m*M* or variable) and quenched after 1.5 min. Both carbamoyl aspartate and dihydroorotate are stable under these conditions.[3] The kinetic parameters were obtained by least squares analysis of the dihydroorotate saturation curves to the Michaelis–Menten equation using the program KaleidaGraph (Synergy Software). The determination of the K_i for the noncompetitive inhibition of DHO by PALA was determined by a least square fit to the equation $V = V_{max}/(1+[PALA]/K_i) + V_f$ where V_f = the maximum DHO inhibition by PALA.

Site-directed mutagenesis

Site-directed mutagenesis to construct the Ala198Arg, Leu199Arg, and Leu200Arg mutants was performed by PCR using Pfu Turbo polymerase (Stratagene) and the plasmid encoding the DHO subunit as a template. The forward and reverse oligonucleotide primers were synthesized by Invitrogen. The fidelity of the constructs was verified by restriction digestion and sequencing.

Peptide synthesis

The peptides were synthesized using a PS3 Automated Peptide Synthesizer from Protein Technologies (Tucson, AZ) using standard solid phase techniques for *N*-α-fluorenylmethyloxycarbonyl (Fmoc) protected amino acids on Rink amide *p*-methylbenzhydrylamine (MBHA) resin (0.64 mmole/g) on a 0.1 mmole scale. This resin produces a C-terminal carboxamide upon cleavage. The side chains of Ser and Glu were protected as the *t*-butyl derivatives and Asn as the trityl form. The deprotection solution for the N-terminal amine was 20% piperidine in *N,N*-dimethylformamide (DMF). o-(Benzotriazol-1yl)-1, 1, 3, 3-tetramethyluronium hexafluorophosphate (HBTU) was used as a coupling agent, activated by 0.4 M N,N-diisopropylethylamine (DIEA) in DMF. Simultaneous deprotection and cleavage from the resin were accomplished by treatment with 10 mL 90% trifluororacetic acid (TFA)/ 10% scavenger cocktail (phenol and water, spiked with a small amount of triisopropylsilane). Crude peptides were purified to homogeneity by preparative reversed-phase high performance liquid chromatography (RP-HPLC) on a Waters (Milford, MA) instrument with a Phenomenex (Torrance, CA) Jupiter C18 column (2.2 × 25.0 cm, 10 mL/min). A linear gradient of 10% acetonitrile (0.1% TFA)/ water (0.1% TFA) to 50% acetonitrile (0.1% TFA)/ water (0.1% TFA) was used, followed by lyophilization. Peptide purity was assessed by analytical RP-HPLC. Peaks were monitored at 214, 230, 254, and 280 nm. The synthesized peptide was ≥97% pure as analyzed by peak integration. Electrospray mass spectrometry confirmed the appropriate molecular weights.

Acknowledgments

We wish to thank Dr. Ruth Ann Armitage (Eastern Michigan University) for providing us with mass spectroscopy data.

References

1. Evans DR, Guy HI (2004) Mammalian pyrimidine biosynthesis: fresh insights into an ancient pathway. J BIol Chem 279:33035–33038.
2. Deckert G, Warren PV, Gaasterland T, Young WG, Lenox AL, Graham DE, Overbeek R, Snead MA, Keller M, Aujay M, Huber R, Feldman RA, Short JM, Olsen GJ, Swanson RV (1998) The complete genome of the hyperthermophilic bacterium Aquifex aeolicus. Nature 392:353–358.
3. Ahuja A, Purcarea C, Ebert R, Sadecki S, Guy HI, Evans DR (2004) Aquifex aeolicus dihydroorotase: association with aspartate transcarbamoylase switches on catalytic activity. J Biol Chem 279:53136–53144.
4. Purcarea C, Ahuja A, Lu T, Kovari L, Guy HI, Evans DR (2003) Aquifex aeolicus aspartate transcarbamoylase, an enzyme specialized for the efficient utilization of unstable carbamoyl phosphate at elevated temperature. J Biol Chem 278:52924–52934.
5. Zhang P, Martin PD, Purcarea C, Vaishnav A, Brunzelle JS, Fernando R, Guy-Evans HI, Evans DR, Edwards BF (2009) Dihydroorotase from the hyperthermophile *Aquifex aeolicus* is activated by stoichiometric association with aspartate transcarbamoylase and forms a one-pot reactor for pyrimidine biosynthesis. Biochemistry 48: 766–778.
6. Christopherson RI, Jones ME (1980) The overall synthesis of L-5,6-dihydroorotate by multienzymatic protein pyr1–3 from hamster cells. Kinetic studies, substrate channeling, and the effects of inhibitors. J Biol Chem 255:11381–11395.
7. Anderson KS, Kim AY, Quillen JM, Sayers E, Yang XJ, Miles EW (1995) Kinetic characterization of channel impaired mutants of tryptophan synthase. J Biol Chem 270:29936–29944.
8. Anderson K (1999) Fundamental mechanisms of substrate channeling. Method Enzymol 308:111–145.
9. Miles EW, Rhee S, Davies DR (1999) The molecular basis of substrate channeling. J Biol Chem 274:12193–12196.
10. Honzatko RB, Crawford JL, Monaco HL, Ladner JE, Ewards BF, Evans DR, Warren SG, Wiley DC, Ladner RC, Lipscomb WN (1982) Crystal and molecular structures of native and CTP-liganded aspartate carbamoyltransferase from *Escherichia coli*. J Mol Biol 160:219–263.
11. Krause KL, Volz KW, Lipscomb WN (1985) Structure at 2.9-A resolution of aspartate carbamoyltransferase

complexed with the bisubstrate analogue N-(phosphonacetyl)-L-aspartate. Proc Natl Acad Sci USA 82:1643–1647.
12. Kantrowitz ER, Lipscomb WN (1990) *Escherichia coli* aspartate transcarbamoylase: the molecular basis for a concerted allosteric transition. Trends Biochem Sci 15: 53–59.
13. Ladjimi MM, Middleton SA, Kelleher KS, Kantrowitz ER (1988) Relationship between domain closure and binding, catalysis, and regulation in *Escherichia coli* aspartate transcarbamylase. Biochemistry 27:268–276.
14. Collins K, Stark G (1971) Aspartate transcarbamylase. Interaction with the transition state analogue N-(phosphonacetyl)-L-aspartate. J Biol Chem 246:6599–6605.
15. Martin P, Purcarea C, Zhang P, Vaishnav A, Sadecki S, Guy-Evans H, Evans D, Edwards B (2005) The crystal structure of a novel, latent dihydroorotase from *Aquifex aeolicus* at 1.7 Å resolution. J Mol Biol 348:535–547.
16. Hyde CC, Miles EW (1990) The tryptophan synthase multienzyme complex: exploring structure- function relationships with X-ray crystallography and mutagenesis. Biotechnology 8:27–32.
17. Anderson KS, Miles EW, Johnson KA (1991) Serine modulates substrate channeling in tryptophan synthase. A novel intersubunit triggering mechanism. J Biol Chem 266:8020–8033.
18. Thoden JB, Holden HM, Wesenberg G, Raushel FM, Rayment I (1997) Structure of carbamoyl phosphate synthetase: a journey of 96 A from substrate to product. Biochemistry 36:6305–6316.
19. Miles BW, Banzon JA, Raushel FM (1998) Regulatory control of the amidotransferase domain of carbamoyl phosphate synthetase. Biochemistry 37:16773–16779.
20. Miles BW, Raushel FM (2000) Synchronization of the three reaction centers within carbamoyl phosphate synthetase. Biochemistry 39:5051–5056.
21. Thoden JB, Phillips GN Jr, Neal TM, Raushel FM, Holden HM (2001) Molecular structure of dihydroorotase: a paradigm for catalysis through the use of a binuclear metal center. Biochemistry 40:6989–6997.
22. Lee M, Chan CW, Guss JM, Christopherson RI, Maher MJ (2005) Dihydroorotase from *Escherichia coli*: loop movement and cooperativity between subunits. J Mol Biol 348:523–533.
23. Lee M, Chan CW, Graham SC, Christopherson RI, Guss JM, Maher MJ (2007) Structures of ligand-free and inhibitor complexes of dihydroorotase from *Escherichia coli*: implications for loop movement in inhibitor design. J Mol Biol 370:812–825.
24. Purcarea C, Martin P, Vickrey JF, Guy HI, Edwards BF, Evans DR (2002) Cloning, expression and preliminary X-ray analysis of the dihydroorotase from the hyperthermophilic eubacterium *Aquifex aeolicus*. Acta Cryst D 58:154–156.
25. Laemmli U (1970) Cleavage of structural proteins during the assembly of the head of bacteriophage T4. Nature 227:680–685.
26. Lowry O, Rosenbrough N, Farr A, Randall R (1951) Protein measurement with the Folin Phenol reagent. J Biol Chem 193:265–275.
27. Prescott LM, Jones ME (1969) Modified methods for the determination of carbamyl aspartate. Anal Biochem 32:408–419.
28. Pastra-Landis SC, Foote J, Kantrowitz ER (1981) An improved colorimetric assay for aspartate and ornithine transcarbamylases. Anal Biochem 118:358–363.